AN ANALYSIS OF MULTIPLE INTERLAMINAR CRACK PROPAGATION UNDER MIXED-MODE DEFORMATIONS

Fabrizio GRECO, Raffaele ZINNO

Department of Structural Engineering, University of Calabria, Cosenza, Italy
f.greco@struct.unical.it; zinno@unical.it

Sommario

Viene presentata un'analisi delle condizioni di inizio e delle caratteristiche del processo di crescita di aree di difetto di adesione interlaminare, situate in prossimità della superficie di piastre laminate composite soggette a compressione. E' presa in esame la presenza di due zone delaminate ipotizzate disposte in modo coassiale sui lati opposti del laminato. Si studia in particolare, l'influenza della dipendenza della resistenza di adesione interlaminare dai "modi" di frattura coinvolti sull'inizio e sulla propagazione del danno da delaminazione.

Abstract

An analysis of the initial conditions and of the characteristics of the growth phenomenon of zones affected by an interlaminar defect, near the external surfaces of laminated composite plates subject to compressive load, is presented in this work. In particular, it is analysed the presence of two delaminated zones coaxially positioned on the two opposite sides of the laminate. It is focused the influence of the dependence of the interlaminar adhesion strength on the fracture modes involved in the appearence and in the growth of the delamination damage.

1. Introduction

Fibre reinforced laminate composites are widely used nowadays in load-bearing structures due to their light weight, high specific strength and stiffness, good corrosion resistance and superb fatigue strength limit. Many successful applications in aerospace, mechanical, naval and, now, also in civil engineering rely on the exploitation of these properties as well as others.

However, like metals, these materials lose much more of their structural integrity when damaged. In particular, laminated composites often present initial delaminations produced from several causes, such us manufacturing imperfections, stress concentrations, object impacts, local or global buckling of laminae.

The presence of interlaminar delaminations may severely reduce the compressive strength of structures made from laminate composite materials. The occurrence of delaminations, in fact,

may allow laminate free surface to buckle locally (delamination buckling phenomenon) thereby creating conditions conducive to delamination growth. Moreover, it is simple to individuate that the main reason of delamination is the poor interlaminar toughness, so it is deducible the importance to develop and to use tougher adhesives or resins to obtain a better connection of the laminate constituting the entire laminate.
The delamination growth phenomenon depends upon the stress state at the crack tip and it is often governed by the mixed-mode stress intensity factor or by the mixed-mode strain energy release rate. This consideration is the main reason of several developed and published research works where are carried out mode I and mode II interlaminar fracture toughness experimental tests or where are developed mixed-mode delamination growth models for composite systems. In this context it is also developed the present work which concerns the behaviour of simple one-dimensional plates subject to compressive loads.
Delamination is assumed to spread from initial interlaminar defects. In particular, the attention is focused on locally buckled laminates containing multiple delaminations as depicted in Fig. 1. The analysis is developed by using an analytical approach based on the Linear Elastic Fracture Mechanics Theory.

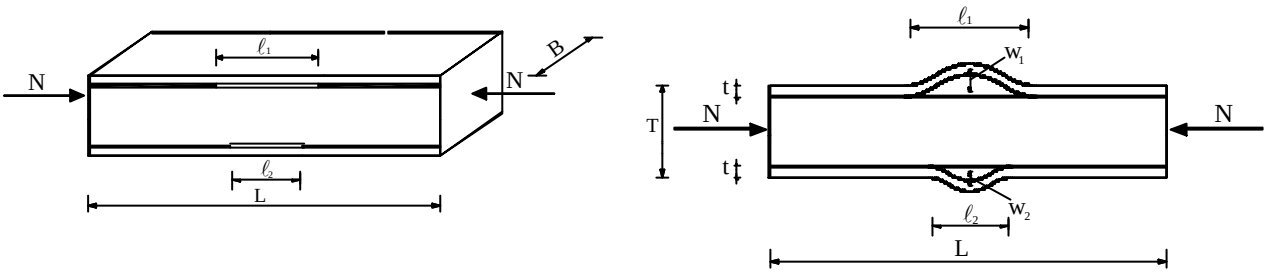

Figure 1 - Locally buckled laminated affected by symmetrically located delaminations

In order to accurately predict the growth of delamination when mode I and mode II are interacting some fracture criteria have been proposed taking into account the experimental evidence. In the present paper, one of these mixed-mode fracture criteria [3] is adopted to obtain important information on mixed-mode fracture behaviour of the laminated one-dimensional plates previously introduced and described.
Some results are given to show the influence on the delamination buckling and on the growth phenomenon of the main geometrical and mechanical characteristics of the structure and to evidence the strong role of the fracture modes on the stable or unstable delamination growth.

2. Multiple delamination analysis for a narrow plate

With reference to the previous Figure 1, here we develop the analysis of the damage evolution produced by a compressive load on a narrow plate subject to two coaxial delaminated zones. The thicknesses of the two external delaminated layers are equal. In particular, the relations governing the mechanical behaviour of the plate after the second critical state are analysed. It is made the hypothesis that the buckling of the second layer appears before the delamination growth initiation of the first buckled layer. The buckling load of the *i-th* layer, in absence of the buckling of the remaining *j-th* layer is:

$$N_{c0i} = \frac{\pi^2}{3}\left(\frac{t_i}{l_{0i}}\right)^2 EBT; \qquad (1)$$

where E is the Young modulus of the homogeneous, linearly elastic, isotropic material constituting the layers. The first buckled layer, obviously, has length (l_{01}) equal or greater than the second one (l_{02}). The following non-dimensional parameters represent the central transverse displacements *(w)*:

$$\boldsymbol{x}_1 = \frac{w\left(\frac{l_1}{2}\right)}{l_1}; \qquad \boldsymbol{x}_1 = \frac{w\left(\frac{l_2}{2}\right)}{l_2}; \qquad (2\text{ a, b})$$

The following post-buckling relations are valid for the first layer [2]:

$$N^{(1)} = N_c^{(1)} + \frac{1}{8} N_c^{(1)} \boldsymbol{x}_1^2; \qquad \frac{u_{l_1}}{l_1} = \frac{N^{(1)}}{EBt} + \frac{\boldsymbol{p}^2}{4}\boldsymbol{x}_1^2 \quad ; \qquad (3\text{ a, b})$$

Because of the hypothesis that layer 2 buckles before the delamination growth initiation of layer 1, and by referencing the compressive load N* as the sum of the $N^{(2)}$ and $N^{(3)}$ relative to the layer 2 and to the core 3, as depicted in Figure 2, for the sublaminate composed by the layer 2 and the core 3, it is possible to write:

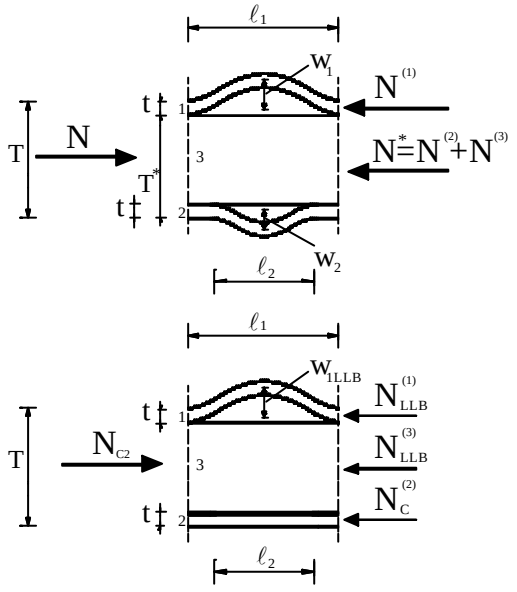

Figure 2 - Layer compressive load distribution

$$\frac{N^*}{N_c^*} = 1 + \left[\frac{1}{8} + \frac{3}{4}\left(\frac{l_2}{t}\right)^2\left(1 - \frac{t}{T-t}\right)\right]\boldsymbol{x}_2^2; \quad (4\text{ a})$$

$$\frac{u_{l_1}}{l_1} = \frac{N^*}{EB(T-t)} + \frac{t}{T-t}\frac{\boldsymbol{p}^2}{4}\frac{l_2}{l_1}\boldsymbol{x}_2^2 \quad ; \qquad (4\text{ b})$$

In the relations (4a, b) N_c^* indicates the value of N* capable to buckle the layer 2:

$$N_c^* = \frac{\boldsymbol{p}^2}{3}\left(\frac{t}{l_2}\right)^2 EB(T-t); \qquad (5)$$

To calculate the value of N_{c2} which is the load which produces the buckling of the second layer, we can observe that $l_1 \geq l_2$.

Moreover, it is possible to write $N_{c2} = N_{LLB}^{(1)} + N_c^*$ where $N_{LLB}^{(1)}$ represents the fraction of N_{c2} adsorbed by the buckled layer 1. Writing the compatibility equations of the axial displacements of the delaminated block as in the figure, and individuating by $N_c^{(2)}$ the buckling load of the layer 2, we can obtain:

$$N_{LLB}^{(1)} = \frac{1 + 6\left(\frac{l_2}{t}\right)^2}{1 + 6\left(\frac{l_1}{t}\right)^2} N_c^{(2)} \quad ; \qquad (6)$$

By substituing relations (6) and (5) into $N_{c2} = N_{LLB}^{(1)} + N_c^*$, it is possible to write:

$$\frac{N_{c2}}{N_{c1}} = Z(l_1, l_2) = \frac{t}{T}\left(\frac{l_1}{l_2}\right)^2 \left[\frac{T-t}{t} + \frac{1+6\left(\frac{l_2}{t}\right)^2}{1+6\left(\frac{l_1}{t}\right)^2}\right]; \qquad (7)$$

where N_{c1} is the buckling load of layer 1, relative to the delamination length l_1, and equal to:

$$N_{c1} = \frac{\pi^2}{3}\left(\frac{t}{l_1}\right)^2 EBT\ ; \qquad (8)$$

By introducing the following ratios between the delamination lengths and the defects lengths:

$$\gamma_1 = \frac{l_1}{l_{01}}; \qquad \gamma_2 = \frac{l_2}{l_{02}}; \qquad k = \frac{l_{02}}{l_{01}}; \qquad k \le 1; \qquad (9\text{ a, b, c, d})$$

we can rewrite equations (7) and (8) as follows:

$$Z(\gamma_1, \gamma_2) = \frac{1}{k^2}\frac{t}{T}\left[\frac{1+6k^2\left(\frac{l_{01}}{t}\right)^2\gamma_2^2}{1+\left(\frac{l_{01}}{t}\right)^2\gamma_1^2} + \frac{T-t}{t}\right]\frac{\gamma_1^2}{\gamma_2^2}; \quad N_{c1} = \left[\frac{\pi^2}{3}\left(\frac{t}{l_{01}}\right)^2 EBT\right]\frac{1}{\gamma_1^2} = \frac{1}{\gamma_1^2}N_{c01}; \quad (10\text{ a, b})$$

To obtain the force-displacement relations we have to impose the compatibility between the axial displacements of the block ends, so by equalizing equations (3b) and (4b) we obtain:

$$N^* = \frac{T-t}{t}N^{(1)} + \frac{\pi^2}{4}EB(T-t)\chi_1^2 - \frac{\pi^2}{4}EBt\,\frac{l_2}{l_1}\chi_1^2\ ; \qquad (11)$$

The total compressive load is $N = N^{(1)} + N^*$, and by using the expressions in eqn. (11) and (3a):

$$\frac{N}{N_{c1}} = 1 + \left[\frac{1}{8} + \frac{3}{4}\left(\frac{l_1}{t}\right)^2\left(1-\frac{t}{T}\right)\right]\chi_1^2 - \frac{3}{4}\frac{t}{T}\frac{l_2}{l_1}\left(\frac{l_1}{t}\right)^2\chi_2^2; \qquad (12)$$

This expression substitutes eqn. (4a) when appears the buckling in the second layer.
By introducing:

$$W = W(l_1) = \frac{1}{8} + \frac{3}{4}\left(\frac{l_1}{t}\right)^2\left(1-\frac{t}{T}\right); \qquad H_2 = H_2(l_1, l_2) = \frac{3}{4}\frac{t}{T}\frac{l_2}{l_1}\left(\frac{l_2}{t}\right)^2; \qquad (13\text{ a, b})$$

it is possible rewrite (12) as:

$$\frac{N}{N_{c1}} = 1 + W(l_1)\chi_1^2 - H_2(l_1, l_2)\chi_2^2; \qquad (14)$$

Moreover, by defining the "fictitious single delaminated body (SD)", obtained from the original laminate by suppressing the second delamination, we can write eqn (12) as follows:

$$\frac{N}{N_{c1}} = 1 + \left[\frac{1}{8} + \frac{3}{4}\left(\frac{l_1}{t}\right)^2\left(1-\frac{t}{T}\right)\right]\chi_{1SD}^2 \;=\; 1 + W(l_1)\chi_{1SD}^2; \qquad (15)$$

By imposing, as previously, the compatibility equations, by using eqns. (3a), (4a) and (5), we reach:

$$\chi_2^2 = R(l_1, l_2)\chi_1^2 - S(l_1, l_2); \qquad (16)$$

where:

$$R(l_1,l_2)=\frac{\frac{1}{8}\left(\frac{t}{l_1}\right)^2+\frac{3}{4}}{\frac{1}{8}\left(\frac{t}{l_2}\right)^2+\frac{3}{4}\left(1-\frac{t}{T-t}\right)+\frac{3}{4}\frac{t}{T-t}\frac{l_2}{l_1}};\quad S(l_1,l_2)=\frac{\left(\frac{t}{l_2}\right)^2+\left(\frac{t}{l_1}\right)^2}{\frac{1}{8}\left(\frac{t}{l_2}\right)^2+\frac{3}{4}\left(1-\frac{t}{T-t}\right)+\frac{3}{4}\frac{t}{T-t}\frac{l_2}{l_1}};$$

or in the other form:

$$\frac{N}{N_{C1}}=1+X(l_1,l_2)+Y(l_1,l_2)\boldsymbol{x}_1^2; \tag{17}$$

with:

$$X=X(l_1,l_2)=H_2(l_1,l_2)S(l_1,l_2);\qquad Y=Y(l_1,l_2)=W(l_1)-H_2(l_1,l_2)R(l_1,l_2);$$

It is also possible to reach, by using the previous relation, the following u_L – N expression:

$$u_L=\frac{NL}{EBT}+\frac{t}{T}\frac{\boldsymbol{p}^2}{4}l_1\boldsymbol{x}_{1SD}^2; \tag{18}$$

In Figures 3 and 4 are depicted the graphical interpretation of the equations (17) and (18).

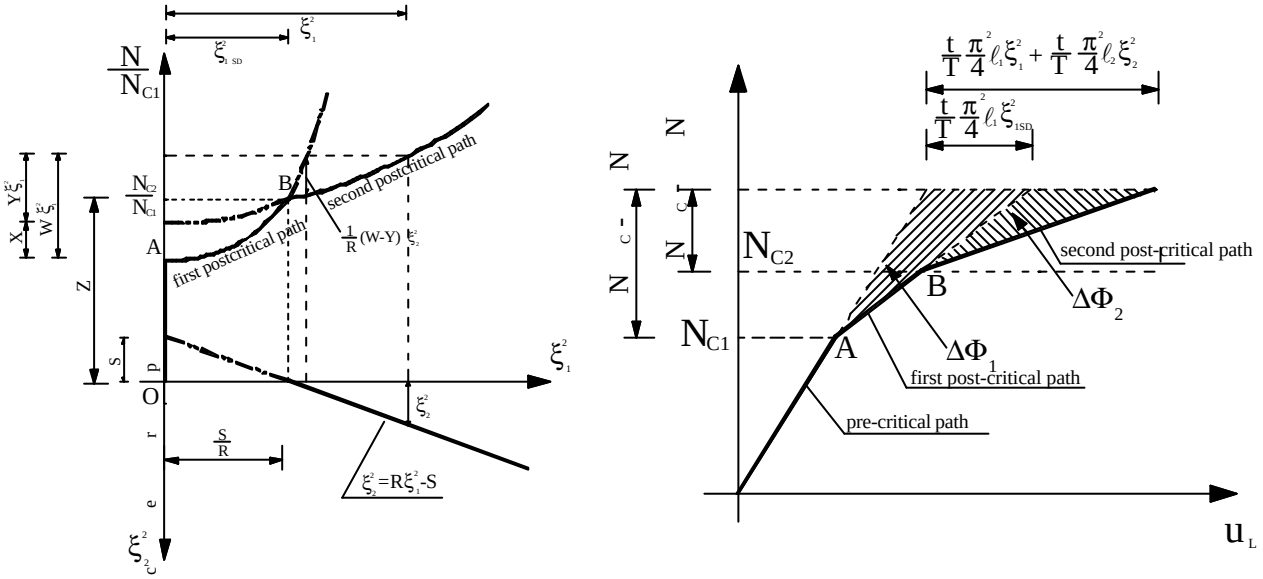

Figures 3, 4 -
Pre and postcritical paths: displacements and potential energy graphical interpretation.

3. Limit equilibrium equations

By remembering the Griffith criterion, the limit equilibrium conditions can be written as:

$$G_1=-\frac{\partial}{\partial l_1}\Delta\Phi=\Gamma B;\qquad G_2=-\frac{\partial}{\partial l_2}\Delta\Phi=\Gamma B; \tag{19 a, b}$$

or, equivalently, using the relations (9 a, b, c, d):

$$-\frac{1}{l_{01}}\frac{\partial}{\partial\Psi_1}\Delta\Phi=\Gamma B;\qquad -\frac{1}{k}\frac{1}{l_{01}}\frac{\partial}{\partial\Psi_2}\Delta\Phi_2=\Gamma B; \tag{20 a, b}$$

In the previous relations $\Delta\Phi_1$, $\Delta\Phi_2$ are the total potential energy increments and Γ is the density of the surface adhesion energy. Observing Figure 4, calculating from it the simple

expressions of $\Delta\Phi_1$ and $\Delta\Phi_2$, so their sum $\Delta\Phi$, and by using the expressions of X, Y, R, S, W, Z previously introduced, we can obtain for equation (19 a):

$$P_1 \hat{l}_1^2 + P_2 \hat{l}_1 + P_3 = 2\alpha_0^{(1)}; \tag{21}$$

where:

$$\alpha_0^{(1)} = \frac{4\Gamma B}{\pi^2 \frac{t}{T} N_{c01}}; \qquad P_1 = P_1(\Psi_1, \Psi_2) = \frac{\partial}{\partial \Psi_1}\left\{\frac{1}{Y}(\Psi_1 + kR\Psi_2)\Psi_1^2\right\};$$

$$P_2 = P_2(\Psi_1, \Psi_2) = -\frac{\partial}{\partial \Psi_1}\left\{\left[\frac{1}{Y}(X+Z+1) - \frac{1}{W}(Z-1)\right]\Psi_1 + k\left[\frac{R}{Y}(X+Z+1) + S\right]\Psi_2\right\};$$

$$P_3 = P_3(\Psi_1, \Psi_2) = -\frac{\partial}{\partial \Psi_1}\left\langle Z\left\{\left[\frac{1}{Y}(X+1) + \frac{1}{W}\left(\frac{1}{Z} - 1\right)\right]\Psi_1 + k\left[\frac{R}{Y}(X+1) + S\right]\Psi_2\right\}\frac{1}{\Psi_1^2}\right\rangle;$$

and for eqn. (19 b):

$$Q_1 \hat{l}_1^2 + Q_2 \hat{l}_2 + Q_3 = 2\alpha_0^{(1)}; \tag{22}$$

where:

$$Q_1 = Q_1(\Psi_1, \Psi_2) = \frac{\partial}{\partial \Psi_2}\left\{\frac{1}{Y}\left[\left(1 - \frac{Y}{W}\right)\Psi_1 + kR\Psi_2\right]\Psi_1^2\right\};$$

$$Q_2 = Q_2(\Psi_1, \Psi_2) = -\frac{\partial}{\partial \Psi_2}\left\{\left[\frac{1}{Y}(X+Z+1) - \frac{1}{W}(Z+1)\right]\Psi_1 + k\left[\frac{R}{Y}(X+Z+1) + S\right]\Psi_2\right\};$$

$$Q_3 = Q_3(\Psi_1, \Psi_2) = \frac{\partial}{\partial \Psi_2}\left\langle Z\left\{\left[\frac{1}{Y}(X+1) - \frac{1}{W}\right]\Psi_1 + k\left[\frac{R}{Y}(X+1) + S\right]\Psi_2\right\}\frac{1}{\Psi_1^2}\right\rangle;$$

The solution of the last two equations (21), (22) gives us:

$$\hat{l}_1 = \hat{l}_1(\Psi_1, \Psi_2); \qquad \hat{l}_2 = \hat{l}_2(\Psi_1, \Psi_2); \tag{23}$$

that in the space $\Psi_1; \Psi_2; l$ represent the limit load surfaces of the two delaminated layers.

4. Modal interaction in symmetrically located delamination growth

The delamination growth has a constrained path (interlaminar). From this descends the observation that the total potential energy is function of the fracture modes involved in the phenomenon. Because of the plane deformation characteristic of the phenomenon , the tearing fracture mode (Mode III) is practically absent. For the two layers (1 and 2) are valid the following:

$$G_1(l, \Psi_1, \Psi_2) = G_{1I} + G_{1II} = \frac{\pi^2}{8}\frac{t}{T} N_{c01}\left(P_1 l^2 + P_2 l + P_3\right); \tag{24}$$

$$G_2(l, \Psi_1, \Psi_2) = G_{2I} + G_{2II} = \frac{\pi^2}{8}\frac{t}{T} N_{c01}\left(Q_1 l^2 + Q_2 l + Q_3\right)\frac{1}{k}; \tag{25}$$

where the adopted symbols are previously introduced. With reference to Figure 5, the following quantities are introduced :

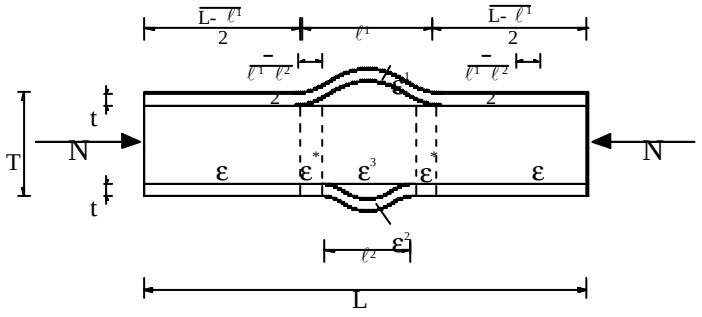

Figure 5- Extensional deformations

$$\varepsilon = \frac{N}{EBT}; \qquad \varepsilon_1 = \frac{N^{(1)}}{EBt}; \qquad \varepsilon_2 = \frac{N^{(2)}}{EBt}; \qquad \varepsilon_3 = \frac{N^{(3)}}{EB(T-2t)}; \qquad \varepsilon^* = \frac{N^{(*)}}{EB(T-t)};$$

The extensional potential energy of the system is:

$$E = E(N, l_1, l_2) = -\frac{1}{2}N\varepsilon(L-l_1) - \frac{1}{2}N^{(1)}\varepsilon_1 l_1 - \frac{1}{2}N^{(2)}\varepsilon_2 l_2 - \frac{1}{2}N^{(3)}\varepsilon_3 l_2 - \frac{1}{2}N^{(*)}\varepsilon^*(l_1 - l_2) =$$

$$= -\frac{B}{2}\left[\varepsilon^2 k(L-l_1) + \varepsilon_1^2 k_1 l_1 + \varepsilon_2^2 k_2 l_2 + \varepsilon_3^2 k_3 l_2 + \varepsilon^{*2} k^*(l_1 - l_2)\right]; \qquad (26)$$

where are adopted the following extensional stiffness parameters:

$$k_1 = Et; \qquad k_2 = Et; \qquad k_3 = E(T-2t); \qquad k^* = E(T-t); \qquad k = ET;$$

The unitary energy release on the delamination front are:

$$G_{1_{II}} = -\frac{\partial E}{\partial l_1} = \frac{B}{2}\left(-\varepsilon_2^2 k + \varepsilon_1^2 k_1 + \varepsilon^{*2} k^*\right) = \frac{B}{2}\frac{k_1 k^*}{k_1 + k^*}\left(\varepsilon^{(1)} - \varepsilon^*\right)^2; \qquad (27)$$

$$G_{2_{II}} = -\frac{\partial E}{\partial l_2} = \frac{B}{2}\left(\varepsilon_2^2 k + \varepsilon_3^2 k_3 - \varepsilon^{*2} k^*\right) = \frac{B}{2}\frac{k_2 k_3}{k_2 + k_3}\left(\varepsilon^{(2)} - \varepsilon_3\right)^2; \qquad (28)$$

From the expressions (27) and (28) it is possible to reach the explicit expressions of G_{1II} and G_{2II} qualitatively similar to the expressions (24) and (25). Moreover, from the relations (24) and (25), by subtracting G_{1II} and G_{2II}, so eqn. (27) and (28), it is possible obtain the expressions for G_{1I} and G_{2I}.

The delamination growth condition, or the limit equilibrium in mixed mode, can be obtained from the expression proposed in [3]:

$$\tilde{G} = G_I + \eta G_{II} = \Gamma B; \qquad \eta = \frac{G_{IC}}{G_{IIC}}; \qquad (29)$$

where G_{IC} and G_{IIC} are the interlaminar strength for mode I and II, respectively. For layer 1 it is possible to write:

$$\tilde{G}_1(l,,\Psi_1,\Psi_2) = G_{1I}(l,,\Psi_1,\Psi_2) + \eta G_{1II}(l,,\Psi_1,\Psi_2) = \Gamma B; \qquad (30)$$

and from here a relation analogous to the equation (21):

$$\tilde{P}_1 \hat{l}_1^2 + \tilde{P}_2 \hat{l}_1 + \tilde{P}_3 = 2\alpha_0^{(1)}; \qquad (31)$$

where $P_i = P_{iI} + \eta P_{iII}$; $(i = 1,2,3)$. The explicit expressions can be obtained in the same way as for P_1, P_2, P_3 in eqn. (21). Analogously for the second layer:

$$\tilde{G}_2(l,,\Psi_1,\Psi_2) = G_{2I}(l,,\Psi_1,\Psi_2) + \eta G_{2II}(l,,\Psi_1,\Psi_2) = \Gamma B; \qquad (32)$$

and from it the equation:

$$\tilde{Q}_1 \hat{l}_1^2 + \tilde{Q}_2 \hat{l}_1 + \tilde{Q}_3 = 2k\alpha_0^{(1)}; \qquad Q_i = Q_{iI} + \eta Q_{iII}; \quad (i = 1,2,3). \qquad (33)$$

in eqns (31) and (33) the coefficient $\alpha_0^{(1)}$ is equal to

$$\alpha_0^{(1)} = \frac{4\Gamma B}{\pi \frac{t}{T} N_{c01}}; \qquad (34)$$

6. Numerical results

When the hypothesis that the buckling of layer 2 precedes, relatively to the initial delamination lengths, the delamination growth onset of layer 1, four situations appears possible:

a) stable path for the delamination of the first layer (for us is the upper layer), while the second one (the bottom layer) is in post-buckling conditions;
b) stable growth for the delamination of the upper layer and no-stable growth for the bottom layer, but stable growth in the "Joined Limiting Equilibrium Load Path (JLEP)" which is the representation of the joined limit equilibrium path in the plane (Ψ_1, Ψ_2) in function of the abscissa *s* where $s : \Psi_1 = k\Psi_2$.
c) no-stable growth for delamination of layer 1, but stable growth in JLEP;
d) stable growth of delamination in both the layers.

In particular, in Figure 6, is depicted the first situation. The light grey surface is relative to the upper layer, while the dark grey is relative to the bottom one. To draw this picture the following values are fixed:

$$k = \frac{l_{02}}{l_{01}} = 0{,}35; \qquad \frac{t}{l_{01}} = 0{,}02; \qquad \frac{t}{T} = 0{,}01; \qquad \alpha_0^{(1)} = \frac{4\Gamma B}{\pi^2 \frac{t}{T} N_{c01}} = 0{,}01;$$

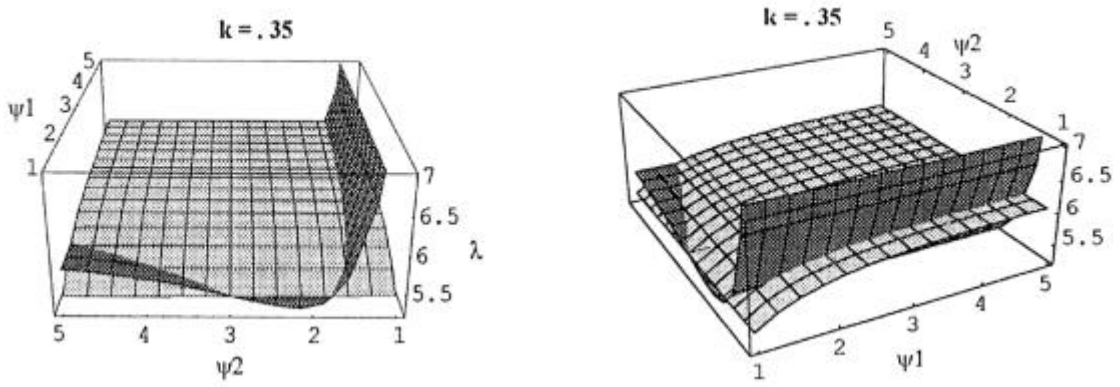

Figure 6 -
Limit surfaces as functions of dimensionless delamination lengths.

5. References

[1] Altus E., Ishai D., *"Delamination buckling criterion for composite laminates: a macro approach"*, Engineering Fracture Mechanics, vol. 41 (5), **1992**

[2] Bruno D., *"Delamination buckling in composite laminates with interlaminar defects"*, Theoretical and Applied Fracture Mechanics, vol. 9 (2), **1988**

[3] Amarg Garg C., *"Delamination – a damage mode in composite structures"*, Engineering Fracture Mechanics, vol. 29 (5), **1988**

[4] Bruno D., Porco G., *"Delaminazione in buckling di piastre laminate"*, Proceedings of the XXIII AIAS National Conference, Rende (CS) 21-24 September, **1994**

[5] Porco G., Zinno R., *"Modal interaction in the debonding problems in laminates"*, Abstract book of "Unilateral problems in Structural Analysis – 5" Conference, Ferrara, 12-14 June, **1997**

[6] Bruno D., Greco F., *"An analysis of mixed mode delamination in plates"*, submitted to Theoretical and Applied Fracture Mechanics, **1999**